Available online at www.sciencedirect.com
SCIENCE DIRECT®
Physica A 331 (2004) 207–218
PHYSICA A
www.elsevier.com/locate/physa

Modelling gaze shift as a constrained random walk

Giuseppe Boccignone[a], Mario Ferraro[b,*]

[a] *Dipartimento di Ingegneria dell'Informazione e Ingegneria Elettrica, Università di Salerno and INFM, via Melillo 1, Fisciano (SA) 84084, Italy*
[b] *Dipartimento di Fisica Sperimentale, Università di Torino and INFM, via Giuria 1, Torino 10125, Italy*

Received 30 July 2003

Abstract

In this paper gaze shifts are considered as a realization of a stochastic process with non-local transition probabilities in a saliency field that represents a landscape upon which a constrained random walk is performed. The search is driven by a Langevin equation whose random term is generated by a Levy distribution, and by a Metropolis algorithm. Results of the simulations are compared with experimental data, and a notion of complexity is introduced to quantify the behavior of the system in different conditions.

PACS: 02.50.Ey; 05.40.Fb; 87.19.Bb; 87.19.Dd

Keywords: Gaze shifts; Levy walks; Complexity

1. Introduction

One of the most interesting areas in mathematical modelling is provided by the processes with which biological visual systems analyze the information coming from the environment; in this paper we present a stochastic model of gaze shifts, eye movements that play an important role in the process of visual information selection. The visual system of primates achieves highest resolution in the fovea—the small (about 1 degree of visual angle) central area of the retina—and the succession of rapid eye movements, known as saccades, compensates the loss of visual acuity in the periphery when looking

* Corresponding author. Tel.: +39-011-6707376; fax: +39-011-6691104.
E-mail addresses: boccig@unisa.it (G. Boccignone), ferraro@ph.unito.it (M. Ferraro).

0378-4371/$ - see front matter
doi:10.1016/j.physa.2003.09.011

Fig. 1. Scanpaths eye-tracked from a human observer, graphically overlapped on the original "Bird" and "Horses" images.

at an object or a scene that spans more than several degrees in the observer's field of view. Thus, the brain directs saccades to actively reposition the center of gaze on circumscribed regions of interest, the so called "focus of attention" (FOA), to extract detailed information from the visual environment. An average of three eye fixations per second generally occurs, intercalated by saccades, during which vision is suppressed. The succession of gaze shifts is referred to as a scanpath [1]. Typical scanpaths of a subject scanning a natural scene are shown in Fig. 1: circles and lines joining circles, graphically represent, respectively, FOAs and gaze shifts between subsequent FOAs.

The selection of the FOA appears to be driven by two different mechanisms: a "bottom up" process which produces rapid scans in a saliency-driven, task-independent manner and a slower "top down" process which is task-dependent and volition-controlled. The degree to which these two mechanisms play a role in determining attentional selection under natural viewing conditions has been for a long time under debate (for an in-depth discussion, see Ref. [2]). Certainly, top-down semantic influences do affect attentional guidance, leading to longer and more frequent fixations on items that are consistent with scene context; individual observers exhibit idiosyncratic scanpaths upon repeated viewings of the same stimulus [1], suggesting that an internal representation is created on initial viewing that guides later reviewing. On the other hand, there exists a strong evidence for stimulus-driven attentional capture, indicating that bottom-up selection can influence attentional allocation in simple experimental paradigms, but there is little research examining the extent of bottom-up attentional allocation under more natural viewing conditions. Recent studies have quantitatively examined the similarity between extracted image features in natural scenes and the fixation locations; in general, measures of edge density and local contrast tend to be greater at the points of fixation than at other locations [2,3].

It is also well known that, beyond the fact that fixations accumulate in visually salient regions, scanpaths connecting salient locations differ among trials [1,4,5]. A number of studies have developed techniques to capture statistical regularities in the pattern of eye scanning. One approach has considered statistical dependencies in parameters such as saccade direction or fixation location [5,6], while other studies have explored the relationship between scanning statistical properties and image statistics [3,7].

Although statistical methods have been applied to analyze data in eye movement research, the specific functional form of saccadic magnitude distributions has attracted

Fig. 2. Saliency maps obtained from images in Fig. 1.

surprisingly little attention. An exception is represented by the work of Brockmann and Geisel who proposed a phenomenological model for the generation of human visual scanpaths [8]. Successions of saccadic eye movements are treated as realizations of a stochastic jump process in a random quenched salience field. Based on the assumption that the visual system minimizes the typical time needed to process a visual scene, the theory predicts that scanpaths are geometrically similar to Levy flights.

The model presented in this paper deals principally with the bottom-up process and relies on a random process to account for stochastic variation in the scanpath sequence exhibited by different observers when viewing the same scene, or even by the same subject along different trials. To this purpose two aspects need to be taken into account: (i) the computation of some measure of saliency over the whole image; (ii) the generation of shifts, to fixate salient points.

As regards the first point, an image can be considered a smooth mapping from a domain $D \subseteq \mathbf{R}^2$ to an m-dimensional range, $\vec{I}: D \to \mathbf{R}^m$; thus the image can be just a scalar field, as in grey-level images, or a vector field, for instance in case of color images, where the three color channels are the vector components. The saliency map is a scalar field obtained through a transformation $\vec{I} \mapsto s(\vec{I}) \in \mathbf{R}$.

Several approaches have been presented in the literature to derive s fields, based on classical image processing algorithms [4], biologically motivated processing [9,10], physics-based transformations [11]. For instance Fig. 2 show the saliency maps obtained from the "Bird" and "Horses" images in Fig. 1 using the approach outlined in Ref. [9] that can be summarized as follows. From color images various conspicuity maps are derived by means of operations known to take place in the visual cortex and are implemented at different spatial scales [12] in a center-surround structure akin to visual receptive fields. Different maps code for the three principal components of primate color vision (intensity, red–green, blue–yellow), and for four orientations (via convolution with Gabor filters). Once all relevant features have been computed in the various maps, they are combined to yield the final saliency map shown in the figure simply by means of a weighted sum of the saliencies of each map. This is basically a pure bottom-up process [10]; however, top–down influences can be taken into account either by modifying such weights using a supervised learning algorithm, and/or by increasing the saliency values on connected sub-domains of the visual field representing the support for specific region of interest (e.g., faces detected by a specialized face detection module).

In most models (e.g., Refs. [4,10]) the s maps determine, in a deterministic fashion, the sequences of gaze shifts: for any given image every scanpath will present the same sequence. On the contrary, here gaze shifts will be considered realizations of a stochastic process with non-local transition probabilities in a saliency field. More precisely, the s-field represents a landscape upon which a constrained random walk is performed, whose steps are generated according to a Levy distribution.

The approach presented here, is somehow akin to models of animal foraging, in the sense that here the visual system looks for areas that are rich in saliency. The advantages of Levy flights versus classical Brownian motion in random searches have been investigated by several authors (see for instance Refs. [13,14]).

2. The model

A general way to combine the dynamical effects of random and deterministic mechanisms is provided by the Langevin equation,

$$\frac{\mathrm{d}}{\mathrm{d}t}\vec{r} = -\vec{\nabla}V(\vec{r}) + \vec{\eta}\,, \tag{1}$$

where V can be modelled as a decreasing function of the saliency field s, for instance

$$V(x, y) = \exp(-\tau_V s(x, y))\,, \tag{2}$$

and $\vec{\eta}$ is a stochastic vector.

Fig. 3 show the V fields obtained applying Eq. (2), with $\tau_V = 0.01$, to the left and right saliency maps shown in Fig. 2, respectively.

In Eq. (1) the stochastic component of the walk is represented by vector $\vec{\eta}$, which is generated by a modified Cauchy–Levy distribution; more precisely, set

$$\begin{aligned} \eta_x &= l\cos(\alpha)\,, \\ \eta_y &= l\sin(\alpha)\,, \end{aligned} \tag{3}$$

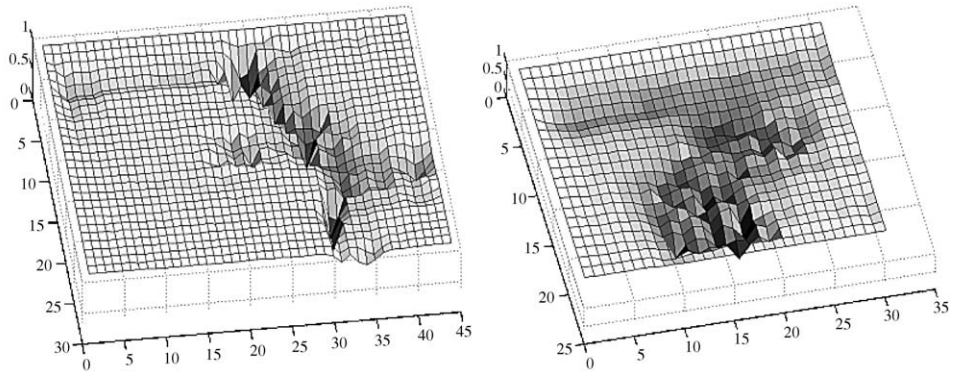

Fig. 3. Potential landscapes obtained from saliency maps shown in Fig. 2.

where the angle α represents the flight direction randomly chosen according to a uniform distribution in the $[0, 2\pi]$ interval.

The jump length l is obtained from the weighted Cauchy–Levy distribution:

$$p(l) = \frac{D\varphi(s)}{l^2 + D^2} \,. \tag{4}$$

The function $\varphi(s)$ modifies the pure Levy flight, in that the probability $p(\vec{r}_{new} \,|\, \vec{r})$ to move from a site $\vec{r}$ to the next site $\vec{r}_{new}$ depends on the "strength" of a bond φ that exists between them [15]. Thus, the jump has a higher probability to occur if the target site is strongly connected in terms of saliency; for any pair $(\vec{r}, \vec{r}_{new})$, $\varphi(s)$ is chosen as

$$\varphi(s) = \exp(-\beta_P(s(\vec{r}) - s(\vec{r}_{new})))\Big/ \sum_{\vec{r}'_{new}} \exp(-\beta_P(s(\vec{r}) - s(\vec{r}'_{new}))) \,, \tag{5}$$

where $\vec{r}$ and $\vec{r}_{new}$ represent the present site and the target site respectively, $\vec{r}'_{new}$ ranges over the set of candidate targets, and the function $s(\cdot)$ their visual saliency.

Next, the jump length l computed according to Eq. (4) undergoes an acceptance process, implemented by a Metropolis algorithm [16]: the flight is accepted according to a probabilistic rule that depends on the gain of saliency and on a "temperature" T, whose values determine the amount of randomness in the acceptance process.

Define the weighted saliency $\hat{s}$ gauged at a fixation center (x_s, y_s) as the Gaussian function

$$\hat{s}(x_s, y_s) = \sum_{x,y \in N} s(x, y) \exp\left(-\frac{(x - x_s)^2 + (y - y_s)^2}{\sigma^2} \right) \,, \tag{6}$$

where N is the support region (FOA neighborhood) centered at (x_s, y_s) whose dimension is modulated by σ (which experimentally can be set to $\frac{1}{6}$ of the smaller value between width or height of the input image [9]). Denote the saliency gain $\Delta\hat{s}$

$$\Delta\hat{s} = \hat{s}(\vec{r}_{new}) - \hat{s}(\vec{r}) \,. \tag{7}$$

Then the target site $\vec{r}_{new}$ is accepted with probability

$$p(a|\vec{r}_{new}, \vec{r}) = \min\{1, \exp(\Delta\hat{s}/T)\} \tag{8}$$

It should be remarked that the stochastic process has been subdivided in two steps—flight generation and acceptance of the new site—for the sake of simplicity, and these two steps together provide a rough computational approximation of a highly complex sensory-motor process, which is far from being fully understood [17]. Note also that the saliency s determines the gaze shift in three different ways: through the term V, by affecting the length of the Levy flight and by deciding the acceptance of the new position.

Fig. 4. Scanpath obtained applying the CLE algorithm at $T = 1.5$.

The random walk performed according to the rules of selection described above, can be so summarized in the following Constrained Levy Exploration algorithm (CLE):

Compute the saliency map $s(\cdot)$ of the image
Compute potential V according to Eq. (2)
Compute φ through Eq. (5)
$\vec{r} \leftarrow$image center; $n \leftarrow 0$
repeat
  Current fixation $\leftarrow \vec{r}$, accepted $\leftarrow false$
  while not accepted **do**
    Generate randomly a jump length l, in a random direction α, with probability $p(l)$ drawn according to Eq. (4)
    Compute $\vec{r}_{new}$ via Langevin Eq. (1)
    Compute $\Delta\hat{s} = \hat{s}(\vec{r}_{new}) - \hat{s}(\vec{r})$
    if $\Delta\hat{s} > 0$ **then**
      Store $\vec{r}_{new}$; $\vec{r} \leftarrow \vec{r}_{new}$; accepted $\leftarrow$ *true*; $n \leftarrow n + 1$
    else
      Generate a random number ρ
      if $\rho < \exp(\Delta\hat{s}/T)$ **then**
        Store $\vec{r}_{new}$; $\vec{r} \leftarrow \vec{r}_{new}$; accepted $\leftarrow$ *true*; $n \leftarrow n + 1$
until $n \leqslant K$

Results from CLE, obtained by solving Eq. (1) through a finite difference scheme with reflecting boundary conditions [18], are shown in Fig. 4 and should be compared with those presented in Fig. 1. The jump length probability, Eqs. (4) and (5), were generated with $\beta_P = 1.0$ and $D = 0.8$; in both images shown in Fig. 4 ($K = 10000$ and $T = 1.5$).

A quantitative comparison between the model and the human data can be provided as follows. First suppose to subdivide the image into N windows and let $p(i)$ be the probability that the gaze is at window i when $t \to \infty$, in other words $p(i)$ is the asymptotic probability distribution. Subregion partitioning of the image, which performs a coarse-graining of the states the gaze can take, is justified by the fact that gaze-shift relevance is determined according to the clustering of fixations that occur in a certain region of the image, rather than by single fixations [4]. Thus, the image was partitioned

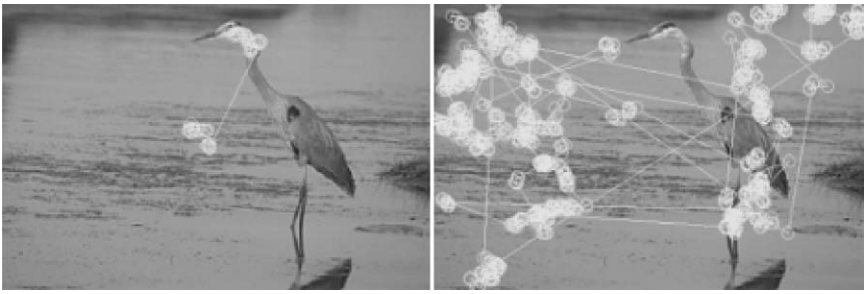

Fig. 5. Scanpath obtained applying the CLE algorithm at $T = 0$ (left), and $T = 15$ (right) to the "Bird" image.

into $N = 16$ rectangular $n \times m$ windows $w(x_i, y_i)$. For all K fixations, each fixation occurring at $\vec{r}_k = (x, y)$, $k = 1 \ldots K$, was assigned to the corresponding window, and probability $p(i)$ was empirically estimated as

$$p(i) \simeq \frac{1}{K} \sum_{k=1}^{K} \chi_{k,i} \ , \tag{9}$$

where $\chi_{k,i} = 1$ if $\vec{r}_k \in w(x_i, y_i)$ and 0 otherwise. This procedure was applied both to human and model generated data, and corresponding probabilities were denoted by p_h, p_m, respectively. Next, the divergence, or distance J was computed [19],

$$J = \sum_{k=1}^{K} (p_h(k) - p_m(k)) \ln \frac{p_h(k)}{p_m(k)} \ , \tag{10}$$

which is used in information theory to quantify the difference between two probability distributions, and in particular has been applied to target recognition issues. With our data Eq. (10) led to a distance $J = 1.62$ for the "Bird" image (Figs. 1 and 2). This value must be contrasted with those obtained by measuring the difference between the p_h distribution and distribution p_m generated by running the simulation at temperatures $T = 0$ and 15 (Fig. 5). In these cases $J = 38.73$ and 58.16, respectively, showing, in agreement with perceptual results, that indeed at $T = 1.5$ the distance between distribution of human scanpath and model generated distribution is small. Similar results have been obtained for the "Horses" image (Figs. 1, 4 and 6), namely $J = 66.44$, 3.32, 45.07 for the same range of temperatures.

3. Measuring scanpath complexity

Consider again images of Figs. 5 and 6, together with those presented in Fig. 4: they show that for increasing T, three kinds of behavior basically occur. In a first low-temperature range, the exploration is trapped in some local potential (left images of Figs. 5 and 6) , while a subsequent range provides normal scanpaths (such as those shown in Fig. 4), and a high-temperature range gives rise to an unconstrained walk

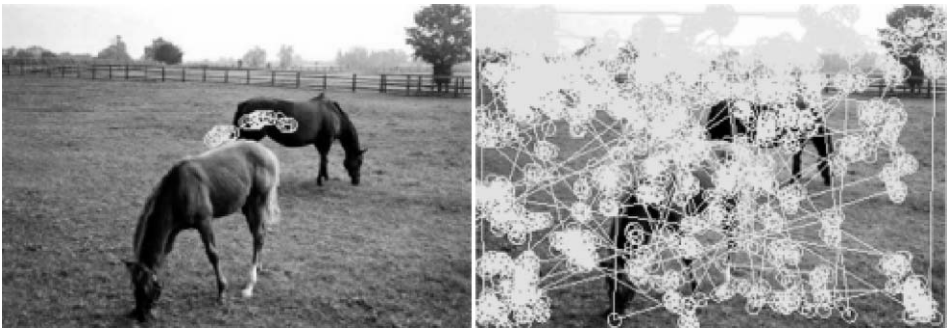

Fig. 6. Scanpath obtained applying the CLE algorithm at $T = 0$ and 15, (left and right images, respectively) to the "Horses" image.

(right images of Figs. 5 and 6). Scanpaths of human observers, then, are situated somewhere in the middle between two extreme cases, as demonstrated by values of the divergence J at different temperatures.

Such a behavior can be given a more precise characterization as follows. Consider the probability distribution p_m. The corresponding Boltzmann–Gibbs–Shannon entropy is $S = -k \sum_{i=1}^{N} p(i) \log p(i)$, where the index m has been dropped for notational simplicity. In the sequel, $k = 1$. The supremum of S is obviously $S_{sup} = \ln N$ and it is associated to a completely unconstrained process, that is a process where s=const, since with reflecting boundary conditions the asymptotic distribution is uniform [20]. Furthermore S is a monotonically increasing function of T since $\lim_{T\to\infty} p(a|\vec{r}_{new}, \vec{r}) = 1$ and the scanpath tends to cover the whole image.

Define, following Shiner et al. [21] a disorder parameter Δ as $\Delta \equiv S/S_{sup}$ and an order parameter Ω as $\Omega = 1 - \Delta$ [21]; complexity Γ is given by

$$\Gamma = \Delta\Omega \,, \tag{11}$$

which ideally is a concave function of T, $\Gamma \approx 0$ for both completely ordered and completely disordered systems, and a has a maximum at some intermediate order/disorder ratio.

Complexity of scanpaths, as a function of T, is depicted in Figs. 7 and 8 that show Γ computed on the "Bird" and "Horses" images, respectively, for increasing temperatures in the range $[0, 15]$, the other parameters being the same used to obtain images in Fig. 4. In a first low-temperature range, the search is mainly affected by the local potential and is trapped at local minima of V and hence Γ is low. When T increases (typically, $T > 1$), the random force becomes more effective in driving the search and scanpath are generated, which are similar to those obtained by human observers; finally, at "temperatures" higher than $T = 10$ the process appears to be driven by the stochastic component and practically unaffected by the saliency of different image regions. Furthermore, when a featureless image is presented in the opposite forms of either a uniform image (no structure) or a random image (random structure), a low complexity of the path should be expected, for any T. This is confirmed by the

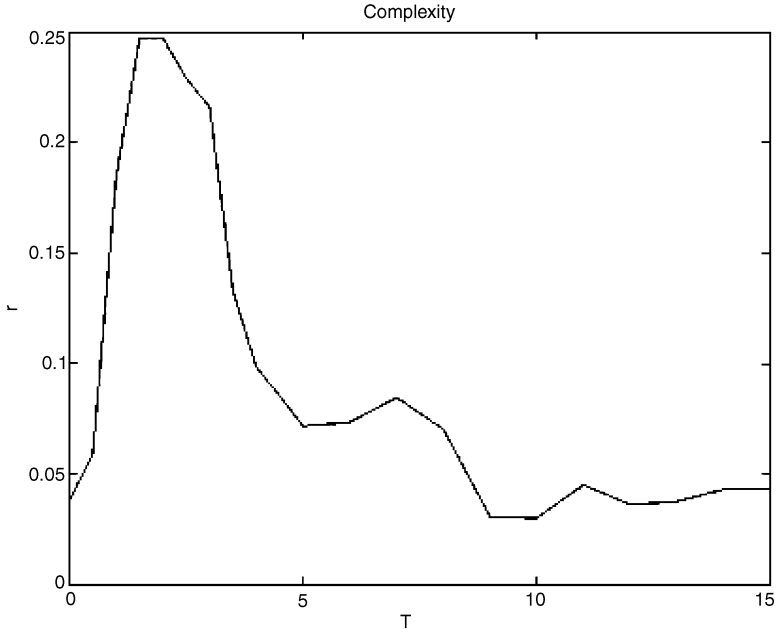

Fig. 7. Complexity curve for the "Bird" image.

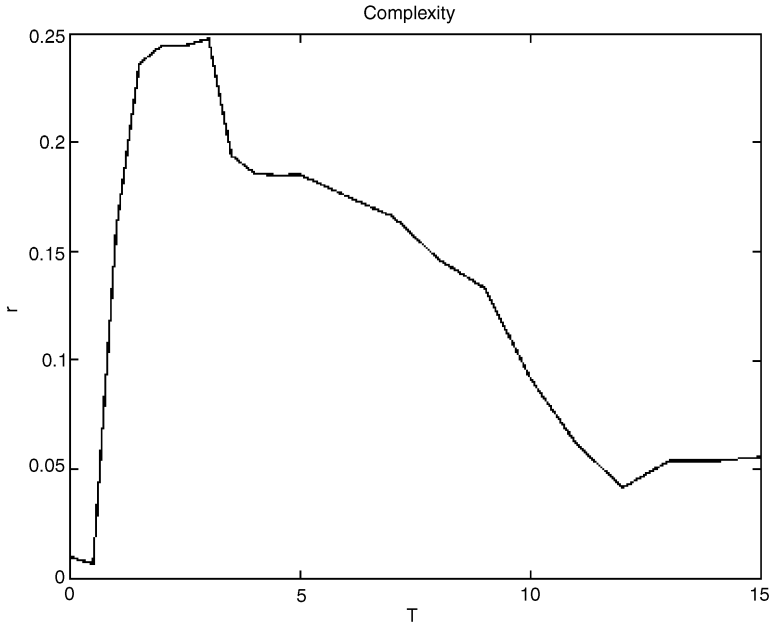

Fig. 8. Complexity curve for the "Horses" image.

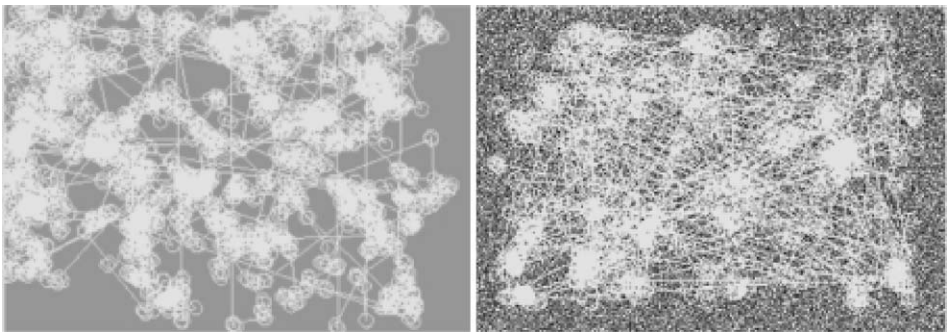

Fig. 9. Scanpath obtained applying the CLE algorithm at $T = 1.5$ to a uniform image and to a randomized version of the horse image.

results of the CLE algorithm; the images shown in Fig. 9 show a sample of scanpaths obtained at $T = 1.5$ for a uniform image, $\vec{I} = const$, and a random image obtained from the "Horses" images by randomly flipping pixel positions. It is worth noting that human observers exhibit a similar behavior: when an uniform or a random images is presented, gaze shifts occur in a random way, independently of observation conditions. In terms of Boltzmann–Gibbs–Shannon entropy, for any given T, values of S are low for images with just a few salient points and increase in case of structured images; the entropy will tend to a maximum when scanpaths explore images without structure, such as uniform or completely random images, where the distribution of the points visited by the gaze is spread over the whole spatial domain. It follows that, for any given T, the complexity Γ of the scanpath is relatively large for images with a rich structure, such as "natural" images, that is images that have a saliency field characterized by several local maxima and it will tend to zero for images that have no definite features or few salient points. This is in accord with the intuitive idea that complexity in a pattern is not a monotonic function of entropy or disorder, but it is small for completely ordered or disordered patterns and has a maximum in between [22].

4. Perspectives

Vision, either biological or artificial, is classically conceived as passive reception of information. For instance, in computational vision the task of vision is generally posed as the transformation of two dimensional data into a description of the three dimensional physical world [23]. However, the assumption that the only function of the visual system is the construction of some sort of internal model or percept of the external world is a quite narrow view of the whole story; indeed the origins of vision may be related more to its contribution to the control of action (such as reaching out and grasping an object) than to its role in conscious perception, a function which appears to be a relative newcomer on the evolutionary scene [24]. There is a growing experimental evidence that vision in human and primates has two distinct and interacting functions: (1) the perception and representation of objects and their relations which

provides the foundations of cognition and (2) the control of actions with respect to the organism's environment [24]. For the purposes of action control only the information that is relevant to behavioral priorities and objectives need to be registered and processed; the brain carries out the selection of information by means of the mechanism of gaze (fixation) shift that, through head and eyes movements, fix the attention on the relevant parts of the scene thus ensuring fast and fluent responses to a changing environment. In this work, it has been shown that gaze shifts, generated by Levy flights over a suitable saliency field reproduce well the results of human observers. The role of the deterministic and stochastic components is clear: the saliency drives the gaze toward the points that are more relevant in the image whereas the large shifts optimize the search in the visual scene. The modelling of gaze shifts through a Levy process over a saliency field can shed light to well known properties of saccadic eye movements such as the phenomenon of inhibition of return (the inhibitory tagging of recently attended location) and, more generally, the random variations of the search process exhibited by different observers when viewing the same scene, or even by the same subject along different trials [4]. Further, Levy distributions of flight lengths, as opposed, for instance, to Gaussian walk, may be essential for optimal search like in optimal foraging, with respect to efficiency, that is the ratio of the number of sites visited to the total distance traversed by the forager [13].

It is worth remarking the role of the potential landscape, derived from the saliency field: different landscapes give rise to different type of walks. Indeed, it has been assumed here that contextual information and top down cues may play a preliminary role in conditioning the formation of the saliency map, thus driving the gaze shift sequence via the deterministic component of the Langevin equation, rather than be explicitly coded as shifting rules. This is consistent with the fact that early stages of visual processing decompose the incoming visual input through an ensemble of feature-selective filtering processes endowed with contextual modulatory effects [10]. The precise nature of this filtering mechanism, which is still subject of investigation and debate (for different hypotheses see, for instance, Refs. [2,25–27]), is not relevant for the model proposed here. However, one could argue, from an evolutionary standpoint, that specific search mechanisms could have been learned and "wired" in order to improve the exploration efficiency (e.g., if a salient point is located within a direct vision distance, maximize the probability of straightforwardly moving to that site).

A measure of the complexity of the process has been provided via the Γ function, which can be thought of as a measure of the information associated to gaze shift, and, in turn, provides a measure of the informational content of the image. Typical methods to measure image information, which usually calculate the Shannon entropy on the image grey-level probabilities, rely on the classical information theory model which assumes the pattern itself as the message source. Here it is offered a different perspective: the message source is not represented by the scene per se, but, rather, by a dynamical system, namely the object/scene observed together with a given transformation, which represent the active observation performed by an agent within a constrained landscape (the world).

The results of the simulations and experimental data indicate that the information gathering mechanism of eye movements works when the system attains the maximum

complexity, in some intermediate state at the edge between complete order and maximum disorder. This result has a simple explanation by considering that in visual exploration, the visual system has to encode the fraction of information, which is useful for behavioral purposes, while an extensive, time-consuming search over the whole visual field may prevent a fast response to the environmental stimuli.

Acknowledgements

The authors would like to thank Dr. Erhardt Barth for providing eye tracking data shown in Fig. 1, Prof. Larry Stark and Prof. Claudio Privitera for enlightening discussions. This research was funded by MURST ex 60% and INFM.

References

[1] D. Noton, L. Stark, Vision Res. 11 (1971) 929.
[2] D. Parkhurst, K. Law, E. Niebur, Vision Res. 42 (2002) 107.
[3] G. Krieger, I. Rentschler, G. Hauske, K. Schill, C. Zetsche, Spat. Vis. 13 (2000) 201.
[4] C. Privitera, L.W. Stark, IEEE Trans. Patt. Anal. Mach. Intell. 31 (2001) 514.
[5] S.R. Ellis, L. Stark, Hum. Factors 28 (1986) 421.
[6] R.D. Rimey, C.M. Brown, Int. J. Comput. Vision 7 (1991) 47.
[7] S.K. Mannan, K.H. Ruddock, D.S. Wooding, Spatial Vision 11 (1997) 157.
[8] D. Brockmann, T. Geisel, Neurocomp. 32/33 (2000) 643.
[9] L. Itti, C. Koch, E. Niebur, IEEE Trans. Patt. Anal. Mach. Intell. 20 (1998) 1254.
[10] L. Itti, C. Koch, Nature Rev. 2 (2001) 1.
[11] M. Ferraro, G. Boccignone, T. Caelli, Pattern Recognition Lett. 23 (2002) 1391.
[12] P.J. Burt, E.H. Adelson, IEEE Trans. Commun. 9 (1983) 532.
[13] G.M. Viswanathan, V. Afanasyevc, S.V. Buldyrev, S. Havlin, M.G.E. Luz, E.P. Raposof, H.E. Stanley, Physica A 282 (2000) 1.
[14] F. Bartumeus, J. Catalan, U.L. Fulco, M.L. Lyra, G.M. Viswanathan, Phys. Rev. Lett. 88 (2002) 097901-1.
[15] M.A.P. Idiart, M. Trevisan, Physica A 307 (2002) 52.
[16] N. Metropolis, A.W. Rosenbluth, M.N. Rosenbluth, A.H. Teller, J. Chem. Phys. 21 (1953) 1087.
[17] R.J. Krauzlis, L.S. Stone, Trends Neurosci. 22 (1999) 544.
[18] R.N. Bhattacharya, E.C. Waymire, Stochastic Processes with Applications, Wiley, New York, 1990.
[19] D. Sheffer, D. Ingman, J. Opt. Soc. Am. A 14 (1997) 1431.
[20] W. Feller, An Introduction to Probability Theory and its Applications, Vol. I, Wiley, New York, 1970.
[21] J.S. Shiner, M. Davison, P.T. Landsberg, Phys. Rev. E 7 (1991) 1459.
[22] P. Grassberger, Int. J. Theor. Phys. 25 (1986) 907.
[23] D. Marr, Vision, Freeman, S. Francisco, CA, 1982.
[24] M.A. Goodale, G.K. Humphrey, Cognition 67 (1998) 181.
[25] Z. Li, Trends Cogn. Sci. 6 (2002) 9.
[26] J.P. Gottlieb, M. Kusunoki, M.E. Goldberg, Nature 391 (1998) 481.
[27] J.K. Tsotsos, S.M. Culhane, W.Y.K. Wai, Y.H. Lai, N. Davis, F. Nuflo, Artif. Intell. 78 (1995) 507.